Experimental Evidence for pK_a-Driven Asynchronicity in C-H Activation by a Terminal Co(III)-Oxo Complex

McKenna K. Goetz and John S. Anderson*

Department of Chemistry, University of Chicago, Chicago, IL 60637, USA

ABSTRACT: C-H activation by transition metal oxo complexes is a fundamental reaction in oxidative chemistry carried out by both biological and synthetic systems. This centrality has motivated efforts to understand the patterns and mechanisms of such reactivity. We have therefore thoroughly examined the C-H activation reactivity of the recently synthesized and characterized late transition metal oxo complex PhB(^{t}BuIm)$_3$Co^{III}O. Precise values for the pK_a and BDFE$_{O-H}$ of the conjugates of this complex have been experimentally determined and provide insight into the observed reactivity. The activation parameters for the reaction between this complex and 9,10-dihydroanthracene have also been measured and compared to previous literature examples. Evaluation of the rates of reaction of PhB(^{t}BuIm)$_3$Co^{III}O with a variety of H-atom donors demonstrates that the reactivity of this complex is dependent on the pK_a of the substrate of interest rather than the BDE$_{C-H}$. This observation runs counter to the commonly cited reactivity paradigm for many other transition metal oxo complexes. Experimental and computational analysis of C-H activation reactions by PhB(^{t}BuIm)$_3$Co^{III}O reveals that the transition state for these processes contains significant proton transfer character. Nevertheless, additional experiments strongly suggest that the reaction does not occur via a stepwise process, leading to the conclusion that C-H activation by this Co^{III}-oxo complex proceeds by a pK_a-driven "asynchronous" concerted mechanism. This result supports a new pattern of reactivity that may be applicable to other systems and could result in alternative selectivity for C-H activation reactions mediated by transition metal oxo complexes.

INTRODUCTION

Transition metal oxo complexes are a remarkable class of intermediates that mediate important C-H activation reactivity in many fields including biology and organic synthesis. As an archetypal example, cytochrome P450 enzymes employ high valent iron oxo species to facilitate the oxidative degradation of pharmaceuticals.[1] Inspired by the success of nature, a variety of synthetic transition metal oxo complexes have been made and their C-H activation reactivity studied thoroughly.[2–5] Transition metal catalyzed C-H activation has also been increasingly investigated as a synthetic strategy, with particular emphasis on controlling selectivity.[6–8] C-H activation by a transition metal oxo complex involves the net transfer of a hydrogen atom and discussion of the intricacies of this transfer has also been a topic of intense interest.[9–13] Understanding this process in detail is crucial for providing a framework for the factors that govern reactivity and selectivity in both natural and synthetic systems.

A broad body of research dedicated to understanding C-H activation by transition metal oxo complexes has established that the reactivity is generally dictated by the thermodynamics of the bond dissociation (free) energies (BD(F)Es) of the C-H bond being broken and the O-H bond being formed. This paradigm, which follows the Bell-Evans-Polanyi principle,[14,15] suggests that in the simplest case, electronic selectivity should be exclusive for the homolytically weakest C-H bond in the substrate.[2,9,16–20] However, net hydrogen atom transfer from an organic substrate to a transition metal oxo complex can occur via multiple possible mechanisms (Scheme 1).[9,21–23] This process involves the transfer of both a proton and an electron which can be transferred simultaneously in a coupled fashion (coupled proton electron transfer, CPET) or stepwise (proton transfer-electron transfer, PTET, or electron transfer-proton transfer, ETPT). It is generally accepted that coupling movement of the proton and electron is energetically favorable; thus, the details of how a proton and electron may couple in these transfers has important implications in C-H activation reactivity.[13,24]

In addition to the limiting extremes mentioned above, it has been proposed that concerted proton and electron

Scheme 1. Mechanisms of net H-atom transfer.

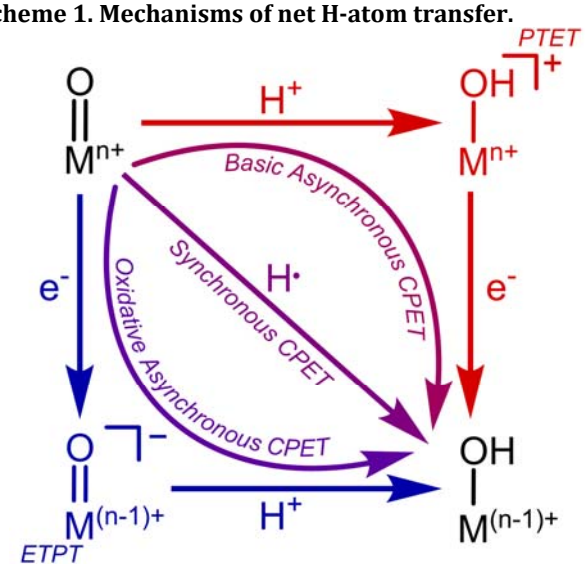

transfer can occur along a spectrum of "asynchronicity" in which the transition state for the net hydrogen atom transfer can contain either more proton transfer or electron transfer character (Scheme 1).[21,23] Computational quantification of this distinction has been newly developed and suggests that more synchronous processes actually have higher activation barriers.[22] This computational proposal has intriguing implications for the selectivity of transition metal oxo mediated C-H activation, but there is a dearth of experimental support for this theory as the vast majority of well-studied oxo complexes display rates which depend on BD(F)Es as discussed above.

There are some limited examples that demonstrate alternative basicity controlled mechanisms of C-H activation.[21,25–28] For instance, Borovik and coworkers report that their $[(H_3buea)Mn^{III}O]^{2-}$ complex activates the weak C-H bond of 9,10-dihydroanthracene by utilizing a PTET mechanism due the high basicity of the Mn^{III}-oxo complex (pK_{aDMSO} = 28.3).[27] The effects of oxo or hydroxo ligand basicity have been invoked in other systems as well. For instance, compensation for low oxidation potentials with increased basicity to maintain a high $BDFE_{O\text{-}H}$ (Equation 1) has been seen in both synthetic and natural systems such as cytochrome P450 enzymes.[17,29–32] Nonetheless "basic asynchronous CPET" has not been studied in a systematic fashion but may be vitally important to these systems.[21,22]

We have recently reported an unusual late transition metal oxo complex $PhB(^tBuIm)_3Co^{III}O$ (**3**, Scheme 2) and preliminary studies of its C-H activation reactivity.[33] In the current work, we have more precisely determined the $BDFE_{O\text{-}H}$ of $PhB(^tBuIm)_3Co^{II}OH$ (**1**, Scheme 2) by explicitly determining the pK_a of $[PhB(^tBuIm)_3Co^{III}OH]^+$ to be ~25.6 in acetonitrile (**2**, Scheme 2). This value makes the corresponding oxo complex, **3**, one of the more basic examples reported in the literature. We have compared these parameters and the reactivity of **3** with 9,10-dihydroanthracene (DHA) to related examples reported in the literature. In addition to these experiments, we have thoroughly investigated the reactivity of **3** with a variety of H-atom donors and found that contrary to the generally established pattern, the reactivity of **3** is dependent on the pK_a of the substrate instead of its $BDE_{C\text{-}H}$. Experimental and computational examination of the transition state provides insight into the mechanism of H-atom transfer in the current system and supports the agency of a basic asynchronous CPET mechanism in the C-H activation reactivity of **3** (Scheme 1). This work represents a clear example of experimental evidence for asynchronicity in C-H activation and opens the door for employing this concept in designing new oxidative reactivity with alternative electronic selectivity.

RESULTS AND DISCUSSION

Thermodynamics

In beginning to examine the C-H activation reactivity in this system, we first sought to accurately determine the BDFE for the O-H bond in **1** using the relationship between pK_a, E^0, and BDFE outlined in Equation 1 and Scheme S1. Previously, cyclic voltammetry data were collected that showed that the Co^{II}/Co^{III} oxidation potential is –0.23 V versus Fc/Fc^+ in acetonitrile (MeCN, Fc = ferrocene, Figure S1).[33] Additionally, a lower bound pK_a value of 26 in MeCN was initially estimated for **2** due to the observation by ^1H NMR spectroscopy that TBD (TBD = 1,5,7-triazabicyclo[4.4.0]dec-5-ene, pK_{aMeCN} = 26.03[34]) was not a competent base for the deprotonation of **2**. Using the C_G value (C_G = standard reduction potential of $H^+/H^\bullet$ in a particular solvent) of 54.9 kcal/mol in MeCN,[9] we calculated an initial lower bound value of 85 kcal/mol for the $BDFE_{O\text{-}H}$ of **1**.

$$BDFE = 1.37pK_a + 23.06E^0 + C_G \quad (1)$$

However, a more accurate value for the $BDFE_{O\text{-}H}$ of **1** was desired to help understand the reactivity of **3** with substrates. To accomplish this, we sought to explicitly determine the pK_a of **2**. This was carried out by titration of **3** with an acid, $[HMTBD][BF_4]$ (MTBD = 7-methyl-1,5,7-triazabicyclo[4.4.0]dec-5-ene, pK_{aMeCN} = 25.49[34]), in MeCN-d_3. The titration was monitored by ^1H NMR spectroscopy at –35 °C where all species in solution (**3**, $HMTBD^+$, **2**, and MTBD) were in rapid equilibrium. As a result, the concentration of each species in solution was evaluated by examination of the observed chemical shift (δ_{obs}) of the methyl protons of $HMTBD^+$/MTBD in the ^1H NMR spectra (See Experimental, Figure S2). From this data, an equilibrium constant for the reaction between **3** and $[HMTBD][BF_4]$ was determined to be 1.2(1) (Table S1). Using the known pK_a value of $[HMTBD][BF_4]$ we calculated a pK_a value of 25.58(5) for **2** in MeCN. We believe the slight discrepancy between this value and our previously determined "lower bound" value is due to hydrogen-bonding effects which complicate interpretation of the acid/base equilibrium with TBD. Using the more precise pK_a value, we calculated a $BDFE_{O\text{-}H}$ of 84.6 kcal/mol (Equation 1, Scheme S1). This value gives a useful benchmark for the types of C-H bonds that might be expected to be activated by **3**.

Scheme 2. Co complexes discussed in this work.

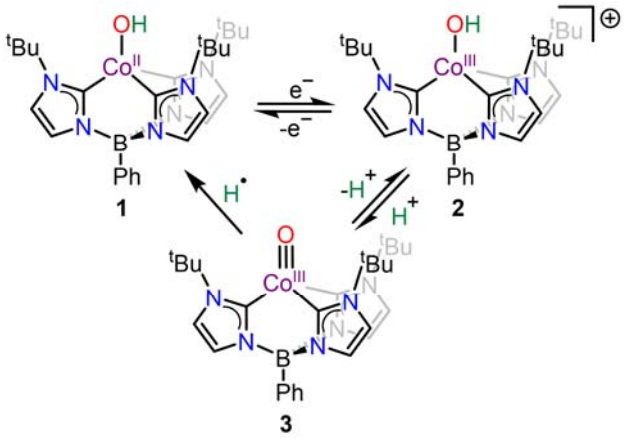

The $BDFE_{O\text{-}H}$ of **1** is comparable to a sample of other well-studied transition metal oxo/hydroxo complexes (Table 1), and it therefore might be expected that **3** would activate C-H bonds analogously to these other species. However, it appears that the balance between pK_a and oxidation potential for the cobalt complex discussed here is weighted in favor of the basicity of the oxo ligand instead of the oxidizing potential of the complex. Additionally, when compared to computed pK_a and E^0 values for a series of non-heme Fe^{IV}-oxo complexes, complex **3** is much more basic and much less oxidizing.[22] This imbalance could affect the mechanism of C-H activation and has been proposed to be a determining factor in asynchronicity.[22]

Table 1. Thermodynamic data for selected transition metal oxo/hydroxo complexes and their reactivity parameters with DHA.

Complex	$\Delta H^{\ddagger}$ (kcal/mol)[a]	$\Delta S^{\ddagger}$ (e.u.)[a]	k_2 ($M^{-1}s^{-1}$)[a]	KIE (k_H/k_D)	pK_a (DMSO)[b]	E^0 (V vs Fc/Fc^+)[c]	$BDFE_{O-H}$ (kcal/mol)	Ref.
$PhB(^tBuIm)_3Co^{III}O$[d]	11(1)	−27(4)	0.0288(7)	10(2)	~15	−0.23	84.6	this work
$[(H_3buea)Fe^{IV}O]^-$[e]	n.r.	n.r.	n.r.	n.r.	11	0.036	87	35
$[(H_3buea)Mn^{IV}O]^-$[e]	5(1)	−49(4)	0.026(2)	6.8	15	−0.11	89	27
$[(H_3buea)Mn^{III}O]^{2-}$[e]	14(2)	−14(6)	0.48(4)	2.6	28.3	−1.51	77	27
$[Fe^{IV}O(TMC)(MeCN)]^{2+}$[f]	n.r.	n.r.	0.14	10	n.r.	n.r.	84(1)	19
$(Cz)Mn^{V}O$[g]	n.r.	n.r.	1.8(5)*10^{-5}	n.r.	~11	−0.33	~80	17
$LCu^{III}OH$[h]	5.4(2)	−30(2)	186	29	~18	−0.076	90(3)	20
$[Ru^{IV}O(bpy)_2py]^{2+}$	n.r.	n.r.	125	35(5)	<−2	>2.2	84.8	36,37
$Fe^{IV}O(TPFPP)$[i]	n.r.	n.r.	13(2)	20	n.r.	n.r.	n.r.	38

[a]Values for reaction with DHA at room temperature. [b]pK_a value for M^{n+}-O/M^{n+}-OH adjusted using the correlation between pK_a values in DMSO, MeCN, THF, and H_2O as necessary. [c]E^0 for M^{n+}-OH/$M^{(n-1)+}$-OH adjusted versus Fc/Fc^+ as necessary. [d]$PhB(^tBuIm)_3^-$ = tris(1-*tert*-butylimidazol-2-ylidene)phenylborate. [e]H_3buea^{3-} = tris[(*N*$_3$-*tert*-butylureayl)-N-ethylene]aminato. [f]TMC = 1,4,8,11-tetramethyl-1,4,8,11-tetraazacyclotetradecane. [g]Cz^{3-} = octakis(para-tert-butylphenyl)corrolazinato. [h]L^{2-} = N,N'-bis(2,6-diisopropylphenyl)-2,6-pyridinedicarboxamide. [i]$TPFPP^{2-}$ = meso-tetrakis(pentafluorophenyl)porphinato. Entries depicting n.r. indicate values not reported to the best of our knowledge.

*Reactivity of **3** with 9,10-dihydroanthracene (DHA)*

As was previously reported, **3** reacts cleanly with DHA to produce **1** and anthracene (Figure 1) under pseudo-first order conditions. Due to the common use of DHA as a model substrate for the C-H activation reactivity of transition metal oxo/hydroxo species (Table 1), we chose to investigate the reactivity of **3** and DHA further. Collecting rate data at variable concentrations of DHA showed a dependence of the rate of reaction on the concentration of DHA, giving a second order rate constant, k_2 = 2.88(7)*10^{-2} $M^{-1}s^{-1}$ (Figure S3, Figure S4). This demonstrates that the reaction follows a second order rate law overall, being first order in [Co] and first order in [DHA]. This k_2 value falls in the middle of the range of other transition metal oxo/hydroxo complexes.

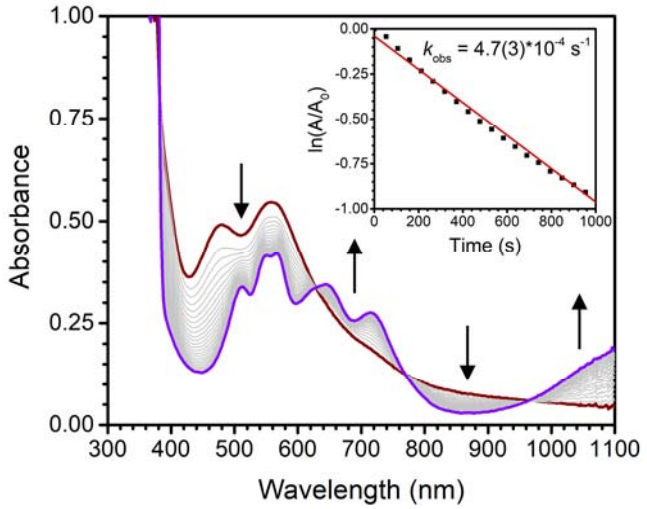

Figure 1. UV-vis spectra of the reaction between **3** (dark red trace) and 10 equivalents of DHA to produce **1** and anthracene (purple trace). Gray traces indicate 1-minute time points. Inset: pseudo-first order kinetic analysis of the reaction monitored at 470 nm.

Additionally, we measured a kinetic isotope effect (KIE) when **3** was reacted with DHA-d_4 of 10±2 (Figure S5). A KIE of this magnitude is common for C-H activation reactions carried out by transition metal oxo/hydroxo species (Table 1) and is slightly beyond the "classical limit" of ~7, implying some degree of contribution from tunneling effects.[39] This is not surprising, given that this reaction involves the overall transfer of both a proton and an electron, but our measured value is far from the extremely high (~30) KIE values determined for some metal oxo/hydroxo complexes.[20] Generally, larger KIE values are consistent with concerted mechanistic processes where the transfer of the electron is intimately coupled to the transfer of the proton, potentially through tunneling. However, KIEs can vary widely depending on the exact nature of the transition state.[13,40–42] This fact makes conclusive interpretation of KIEs difficult.

Finally, we sought to determine the activation parameters, $\Delta H^{\ddagger}$ and $\Delta S^{\ddagger}$, for the reaction between **3** and DHA. This information has been reported for some transition metal oxo/hydroxo complexes that react with DHA, allowing for comparison of our system to those previously reported. Collection of rate data at various temperatures and fitting using the Eyring equation (Figure S6, Figure S7) gave the values $\Delta H^{\ddagger}$ = 11(1) kcal/mol and $\Delta S^{\ddagger}$ = −27(4) e.u. The negative entropy of activation is consistent with a bimolecular transition state in which two species must come together for the reaction to proceed. Such a transition state would be consistent with any of the mechanistic reaction pathways laid out in Scheme 1 and cannot be used to distinguish between them. The activation parameters determined for **3** are typical in the series of transition metal oxo/hydroxo complexes shown in Table 1, with activation enthalpies between 5 to 15 kcal/mol and activation entropies between −15 to −50 e.u.

H-atom transfer reactivity with substrates

Table 2. Kinetic data for the reaction of 3 with various C-H substrates.

Substrate	k_{obs} ($10^{-4}s^{-1}$)[a]	k_2 ($10^{-2}M^{-1}s^{-1}$)	KIE (k_H/k_D)	pK_a (DMSO)[b]	BDE_{C-H} (kcal/mol)[c]
9,10-dihydroanthracene[d]	4.7(3)	2.88(7)	10(2)	30.1	76.3
xanthene	7.2(2)	n.d.	n.d.	30.0	75
1,1,3,3-tetraphenylpropene	0.21(9)	n.d.	n.d.	25.8	77
diphenylmethane	0.16(3)	0.009(2)	n.d.	32.3	84.5
1,3-cyclohexadiene[d]	0.22(13)	0.032(6)	n.d.	35	74.3
9-X-9*H*-fluorene					
X = H	43(2)	24(3)	3.2(3)	22.6	82
^{t}Bu	2.8(4)	n.d.	n.d.	24.4	79.9
Ph	950(90)	n.d.	n.d.	17.9	74

[a]Determined using 10 equivalents of substrate per equivalent of Co complex either directly or from the k_2 value. [b]Data taken from the Bordwell pK_a table.[43] [c]Data taken from the CRC's Handbook of Bond Dissociation Energies.[44] [d]Rates corrected for stoichiometry. Entries depicting n.d. indicate values that were not determined.

As was mentioned above, the general trend in reactivity for transition metal oxo complexes with various H-atom donors is that substrates with stronger C-H bonds react more slowly.[9,17] In an effort to investigate whether or not the reactivity of complex **3** follows this same trend, we examined the reactivity of **3** with a series of H-atom donors with different BDE_{C-H} values (Figures S8-S18) and the results of these studies are presented in Table 2 as observed rate constants (k_{obs}). All of these reactions demonstrate isosbestic conversion from **3** to **1** by UV-vis spectroscopy (Figure 1). Additionally, the reactions of **3** with DHA and fluorene were examined by GC-MS and the expected products of the reaction (anthracene and 9,9'-bifluorenyl, respectively) were observed with 75-100% conversion (Figure S19, Table S2), supporting the clean transformations seen by UV-vis spectroscopy.

Surprisingly, when the kinetic data are plotted as the log(k_{obs}) versus BDE_{C-H} of substrate (Figure 2A) no discernible correlation between the BDE_{C-H} of the substrate and the rate of reactivity is observed. This is contrary to what might be expected based on literature precedent. As a particularly illustrative series, the reactivity of **3** with 1,3-cyclohexadiene (CHD), DHA, and fluorene shows an inverse relationship with BDE_{C-H}. To explain this discrepancy, we considered additional parameters that could correlate with reactivity. Two likely thermodynamic parameters are the pK_a or E^0 of the C-H substrate. Such parameters might be expected to dictate the reactivity if the mechanism were stepwise or asynchronous (Scheme 1). Plotting the log of the k_{obs} values versus the gas phase ionization energies (Figure S20) shows little correlation between these two quantities, as might be expected due to the low oxidation potential of our system. Alternatively, examination of a plot of the log of the k_{obs} values versus the pK_a of each substrate (Figure 2B) reveals a linear correlation where substrates with higher pK_a values react with slower rates. It is prudent to note that while there is a definitive correlation between the rate of C-H activation and the pK_a of the substrate being studied, there are a few substrates that deviate from the line. Most notable in this regard are 9-(*tert*-butyl)-9*H*-fluorene and 1,1,3,3-tetraphenylpropene. Both of these substrates contain tertiary C-H bonds, likely introducing steric clashing with the three *tert*-butyl groups that surround the Co-O bond in **3**. We argue that this steric effect likely leads to aberrantly slow observed rates for these substrates.

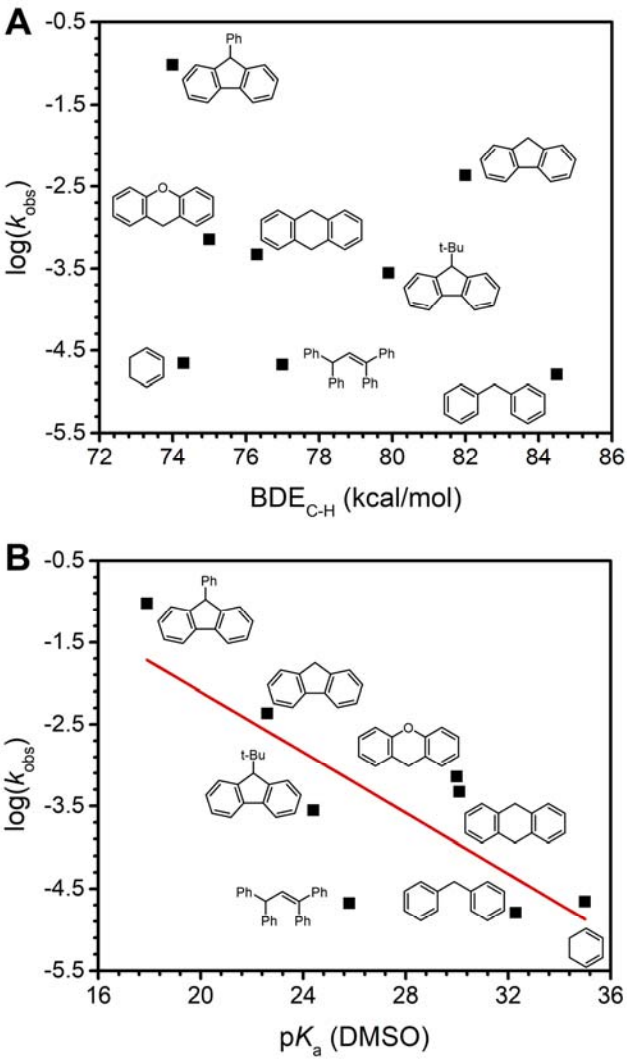

Figure 2. Plots of log(k_{obs}) vs (A) BDE_{C-H} of substrate and (B) pK_a of substrate. Each k_{obs} value is that for the reaction of **3** with 10 equivalents of substrate either determined directly or from the k_2 value (see Experimental and Supporting Information). Linear fit in (B): log(k_{obs}) = –0.18pK_a + 1.6, R^2 = 0.56.

This correlation with pK_a of the substrate suggests a basicity-controlled mechanism of H-atom transfer and could be consistent with a stepwise transfer of the proton and electron (PTET mechanism) or a concerted mechanism in which the transition state contains a significant amount of proton transfer character (i.e. basic asynchronous CPET). Stepwise C-H activation has been observed previously in the literature,[27,28] with one well-studied example being the reactivity of a Mn^V-imide complex with substituted phenol substrates reported by Abu-Omar and coworkers. In this study, it was found that for acidic enough substituted phenols, the data were consistent with a stepwise PTET mechanism, while for the more basic substituted phenols, the data were consistent with a CPET process.[28] On the other hand, asynchronous mechanisms of hydrogen atom transfer have also been proposed in some systems.[21,22] We therefore set out to distinguish between these two mechanisms.

*Mechanism of C-H activation by **3***

In order to better understand the mechanism of C-H activation employed by **3**, we turned to various experimental techniques for studying the characteristics of the transition state of this reaction. Hammett analysis is a powerful technique in this regard that informs on the type of charge build-up on the atom of interest in the transition state. In this instance, we are probing the character of the charge build-up on the carbon of the C-H bond being broken. We therefore carried out Hammett analysis for *p*-substituted 9-phenyl-9*H*-fluorenes. It has been shown previously that for a synchronous CPET process, a negative Hammett correlation is expected.[17] However, for mechanisms such as PTET or basic asynchronous CPET a positive Hammett correlation would be expected due to the build-up of negative charge.

The results of the Hammett analysis (Figures S21-S23) are summarized in the first half of Table 3 and graphically represented in Figure 3. There is a positive Hammett correlation with $\rho = 0.67(7)$. This positive slope supports our hypothesis that the reactivity of **3** with H-atom donors is proton-controlled, consistent with either a stepwise PTET or basic asynchronous CPET mechanism. While this trend is clear in this series, we also wanted to carry out this analysis for another class of substrates with C-H bonds at the upper end of the pK_a range studied due to the fact that the substituted phenylfluorenes are relatively acidic (pK_a ~19 in DMSO). Thus, we chose to look at 3-substituted xanthenes

Table 3. Rates for substrates used in Hammett analyses.

Substrate		k_{obs} (10^{-3} s^{-1})[a]	σ_p^- [b]
9-(4-X-phenyl)-9*H*-fluorene			
X =	OMe	54(1)	–0.26
	Me	66(1)	–0.17
	H	95(9)	0.00
	CF_3	200(30)	0.65
3-X-xanthene			
X =	Me	0.22(2)	–0.17
	H	0.72(2)	0.00

[a]Values obtained using 10 equivalents of substrate. [b]Hammett parameters obtained from Hansch, Leo, and Taft.[45]

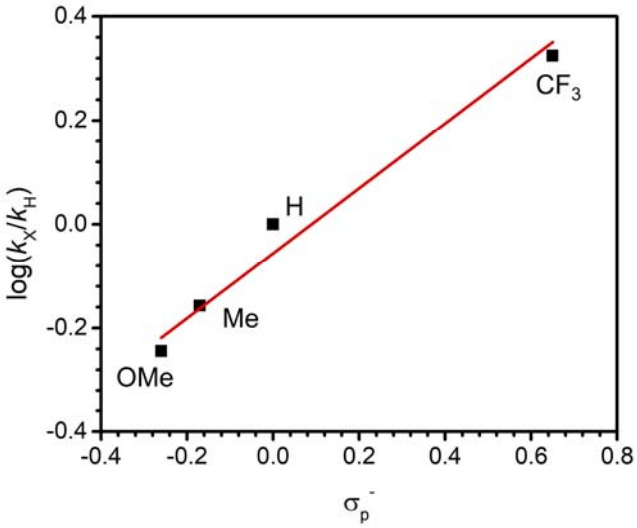

Figure 3. Hammett substituent plot for the reaction of 3 with 9-(4-X-phenyl)-9H-fluorenes. The red line shows the linear fit of the data: $\rho = 0.67(7)$, $R^2 = 0.96$.

(pK_a ~ 30 in DMSO). However, due to synthetic challenges in obtaining three or more 3-substituted xanthene substrates, kinetic analysis was carried out only with 3-methylxanthene (Figure S24) and xanthene and we were unable to obtain a meaningful Hammett slope. Nonetheless, if this class of substrates is reacting via the same mechanism as the *p*-substituted 9-phenyl-9*H*-fluorene derivatives, it would be expected that 3-methylxanthene would react at a slower rate than xanthene. Indeed, this is what was observed, with the rate of reaction for 3-methylxanthene being ~3x slower than that for xanthene (Table 3). Thus, we can say with confidence that these two classes of substrates appear to be reacting via the same basicity-controlled mechanism despite the large (~12 log units) difference in pK_a between the two. This supports the assertion that the same mechanism is operative for all substrates studied in this work.

In addition to the KIE data discussed earlier for DHA, we also determined the KIE for fluorene (Figure S18, Table 2). As has been previously established,[39] large KIE values beyond the classical limit of ~7 are indicative of contributions from tunneling effects, a common observation with transition metal oxo complexes that activate C-H bonds via synchronous CPET. We observed such a KIE with DHA (KIE = 10(2)) which indicated to us that there may be some contribution from tunneling. However, in the case of the more acidic fluorene, we observed a KIE of 3.2(3) which is well within the classical limit. As noted above, it is difficult to interpret KIE values without a detailed picture of the transition state.[13,40–42] Nevertheless, we can propose a speculative interpretation of these comparative values. The observed KIEs could suggest that a stepwise PTET mechanism is operative for fluorene and there is a pK_a-dependent mechanism switch as seen in the Mn^V-imide system.[28] Alternatively, this difference in KIE values may be explained by one asynchronous CPET mechanism where a larger degree of asynchronicity results in a smaller KIE (i.e. the proton is less coupled to the electron).[22] The reaction between **3** and fluorene would be expected to be more asynchronous than that between **3** and DHA due to the smaller pK_a difference between **3** and fluorene.

Scheme 3. Possible mechanisms of C-H activation by complex 3.

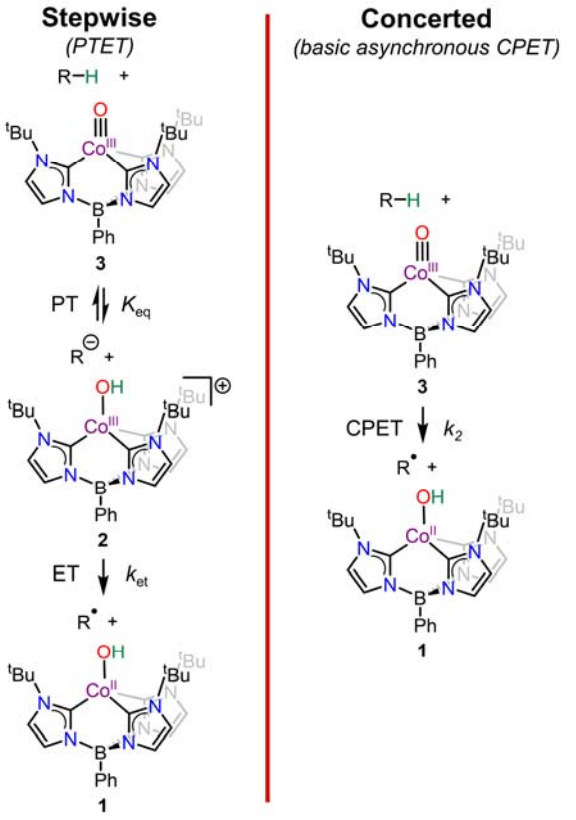

All of the experimental data presented above support that proton transfer plays an integral role in the C-H activation reactivity of **3**, but these experiments cannot discern between a stepwise or concerted mechanism. As discussed above, we envision two likely mechanistic scenarios (Scheme 3). Firstly, one plausible possibility is a PTET mechanism where a pre-equilibrium PT to generate **2** and substrate anion is followed by ET to result in net H-atom transfer. Secondly, an alternative pathway where a basic asynchronous CPET is operative may also be feasible. Experimentally distinguishing between these two mechanisms is difficult, but we reasoned that if **2** were a genuine intermediate in the reactivity of **3**, we should be able to show that this species is kinetically competent to carry out the reaction and that we might be able to intercept it in some way to verify its agency.

It is reasonable to assume that the stepwise mechanism shown in Scheme 3 would occur under steady-state conditions. This imposes a k_{et} (homogeneous electron transfer rate constant) value for the electron transfer between **2** and the substrate carbanion that can be determined from the measured k_2 value for a given reaction and the pK_a difference between the substrate and **2** (See derivation in the SI). Taking fluorene as an example substrate, a k_{et} value of $\sim 10^6$ $M^{-1}s^{-1}$ at room temperature is required to be in agreement with the experimentally determined kinetics.

We can estimate the upper bound of k_{et} by measuring the intrinsic ability of **1**/**2** to give up/accept an electron using cyclic voltammetry (CV) and analyzing the change in ΔE_p with varying scan rate.[46] This measurement gives a k_s value (the heterogeneous electron transfer rate constant) which can be correlated to k_{et} given the assumption that $\Delta G^{\ddagger}$ changes negligibly from heterogeneous to homogeneous conditions, as has been previously shown.[47] We conducted this measurement (Figures S25-S27, see Experimental for mathematical details) and found that the upper bound k_{et} for **1**/**2** is on the order of 10^3 $M^{-1}s^{-1}$ at room temperature. Based on this analysis, it is clear that **2** cannot accept an electron fast enough to match the measured kinetics for the reaction of **3** and fluorene (Table 2). This provides evidence against a stepwise PTET mechanism of C-H activation (Scheme 3).

We also attempted to intercept **2** to see if it were a bona-fide intermediate in the C-H activation reactivity of **3**. Given the steady-state approximation discussed earlier, it might be expected that in the presence of an appropriate deuterated acid, such as [DMTBD][BF_4], scrambling of deuterium into the organic product and the excess substrate would occur due to the presence of **2** and the substrate carbanion in solution. This hypothesis hinges on the equilibrium exchange being appropriately fast while the electron transfer rate from **2** to the carbanion is suitably slow. We can estimate a lower bound for the rate of equilibrium proton exchange from the pK_a determination experiment described above, where the peaks in the ^{1}H NMR spectrum were fully coalesced at −35 °C. This implies a minimum rate of exchange on the order of 10^2 s^{-1} at this temperature.[48] From the room temperature experimentally estimated k_{et} presented above, we can expect that k_{et} at −35 °C should be on the order of 10^1 $M^{-1}s^{-1}$ (See Experimental). Thus, we can reasonably expect to observe deuterium incorporation if a pre-equilibrium is involved in the mechanism of C-H activation.

We carried out the scrambling experiment by reacting **3** with fluorene in the presence of excess [DMTBD][BF_4] and MTBD at −35 °C and evaluating the organic products by GC-MS to test for deuterium incorporation. Comparison of the mass spectra of both fluorene and 9,9'-bifluorenyl in the reaction mixtures with and without added deuterated acid reveals no deuterium incorporation in any of the fluorene-derived species (Figure S28). This observation strongly implies that there is no buildup of **2** or substrate carbanion in the reaction mixture and thus supports a concerted net H-atom transfer mechanism, in this case basic asynchronous CPET.

Computational analysis

While these experimental results are consistent with a concerted asynchronous process, we also wanted to obtain computational support for this pathway. We have performed two sets of DFT studies to probe these C-H activation reactions in detail. Firstly, we followed the procedure laid out by Srnec and coworkers for calculating the asynchronicity parameters, η, for the reactions of **3** with CHD, DHA, and fluorene (Table S3).[22] The value η is a parameter that quantitatively informs on the relative thermodynamic contributions of pK_a and redox potential to the driving force for a net H-atom transfer reaction. A negative η value implies that the pK_a is the dominant driving force whereas a positive η value implies that the redox potential is dominant. Additionally, a larger magnitude of η demonstrates a greater imbalance of the contributions of pK_a and redox

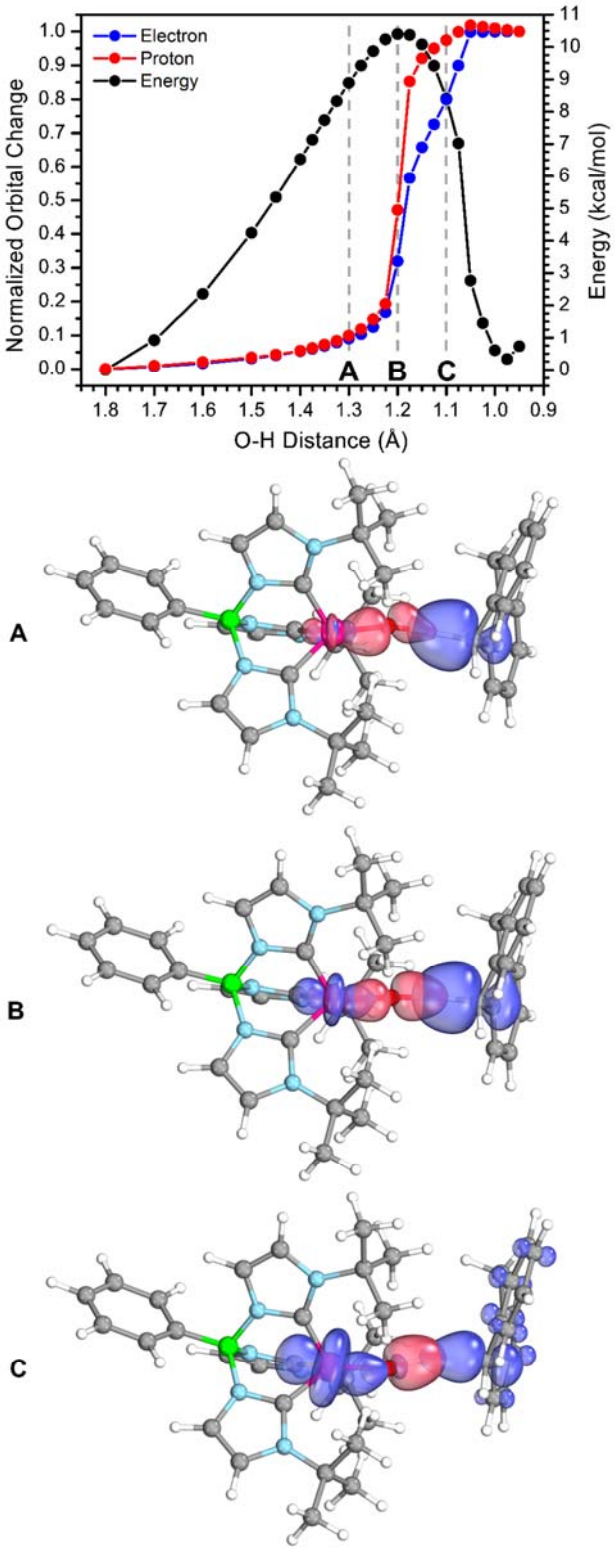

Figure 4. IBO analysis showing the normalized orbital movements involved in the proton transfer (red) and the electron transfer (blue). A, B, and C indicate the stationary points at O-H distances of 1.3, 1.2, and 1.1 Å respectively with the blue orbital involved in the electron transfer and the red orbital involved in proton transfer.

potential to the driving force which results in a propensity for asynchronicity in the H-atom transfer reaction. In the current system, all three of the computed η values are negative, implying that the reactions proceed via asynchronous mechanisms with proton transfer character in the transition state. Additionally, η becomes more negative as the pK_a of the substrate decreases, indicating that the reaction is more asynchronous for more acidic substrates. Finally, it is worth noting that the k_2 values reported in Table 2 trend logarithmically with η (Figure S29), with faster rates of reactivity seen for more asynchronous processes. These results are consistent with the theory of asynchronicity as laid out by Srnec, supporting the idea that lower barriers resulting from higher degrees of asynchronicity lead to faster rates of reactivity, which is observed experimentally in our system.

Secondly, we analyzed the reaction coordinate for C-H activation. As a starting point, we note that while both starting materials are singlets, we have been unable to locate a maximum along a singlet spin manifold. Instead, a maximum is observed along a triplet spin surface (Figure 4). The overall reaction to form **1** and the organic radical mandates a net spin change from $S = 0$ to $S = 1$ (or potentially $S = 2$ if the radical couples ferromagnetically) so the relevance of multiple spin manifolds is not surprising. The relative importance of different spin manifolds has been extensively invoked in transition metal oxo C-H activation reactivity as well as in the reactivity of related Fe carbene systems.[49–51] While we have largely focused this discussion on probing the relative importance of an asynchronous C-H activation mechanism, we acknowledge that the involvement of multiple spin states is a convolution that we have not yet thoroughly addressed.

To obtain further detail on the flow of protons and electrons along the reaction coordinate and in the transition state, we employed an intrinsic bond orbital (IBO) analysis as reported by Knizia and coworkers and recently applied to C-H activation by Fe-oxo complexes (Figure 4, Figure S30).[52–54] This computational technique enables analysis of the movement and localization of orbitals along a reaction coordinate. This allows us to visualize and quantify how the orbitals associated with electron transfer (Figure 4, blue orbital) and proton transfer (Figure 4, red orbital) change as the O–H bond forms. This analysis clearly indicates that both protons and electrons move along the reaction coordinate in a coupled manner. To further test the concept of asynchronicity, we plotted the normalized orbital movement as a function of the O-H distance along the reaction coordinate (Figure 4). This analysis supports that the proton and electron move in a concerted manner, but also shows that the degree of proton movement is greater than the degree of electron movement at intermediate steps along the reaction coordinate. This observation is consistent with the concept of asynchronicity and supports our overall picture of the reaction and experimental results.

CONCLUSIONS

We have presented a thorough study of the C-H activation reactivity carried out by a Co^{III}-oxo complex and have determined that this reactivity occurs via basic asynchronous CPET. DFT calculations and experimental evidence indicate that the reaction does not employ a stepwise mechanism and the dependence of the rate on the pK_a of the substrate indicates that proton movement is paramount. This is in direct contrast to the vast majority of previous systems where the reactivity is controlled by the substrate $BDE_{C\text{-}H}$. While

such proton-controlled reactivity has been observed previously, these systems have invoked stepwise PTET mechanisms to explain their observations. To the best of our knowledge, this is the first example demonstrating experimental evidence for asynchronicity in C-H activation. This asynchronous pathway offers a compelling alternative to mechanisms that have been traditionally invoked. For instance, a basic asynchronous mechanism would imply selectivity for the most acidic C–H bond in a substrate as opposed to the homolytically weakest bond. Furthermore, asynchronous mechanisms may be relevant in a number of processes, as potentially indicated by the important role of basicity noted in cytochrome P450 enzymes.[29] This observation could open the door to new selectivity in reactions carried out by transition metal oxo complexes and adds to our growing understanding of C-H bond activation.

EXPERIMENTAL

Materials and Instrumentation

All manipulations were performed under a dry nitrogen atmosphere using either standard Schlenk techniques or in an mBraun Unilab Pro glovebox unless otherwise stated. All chemicals were obtained from commercial sources and used as received unless otherwise stated. Solvents were dried on a solvent purification system from Pure Process Technologies before storing over 4 Å molecular sieves under N_2. Tetrahydrofuran (THF) was stirred over NaK alloy and passed through a column of activated alumina prior to storing over 4 Å sieves under N_2. 9,10-dihydroanthracene, and xanthene were recrystallized from hexanes and fluorene and diphenylmethane were recrystallized from methanol prior to use. 1,3-cyclohexadiene was distilled and stored over 4 Å molecular sieves prior to use. DHA-d_4 was prepared according to a literature procedure and recrystallized prior to use.[55] All other substrates were synthesized using slightly modified literature procedures (see below). PhB(^{t}BuIm)$_3$Co^{III}O was synthesized according to the previously reported procedure using potassium hexamethyldisilazide as the base.[33] UV-vis spectra were recorded on a Thermo Scientific Evolution 300 spectrometer with the VISIONpro software suite. The UV-vis spectra for the reaction of **3** with 9-(4-(trifluoromethyl)phenyl)-9*H*-fluorene were recorded using an Agilent HP 8453 spectrometer with the UV-vis ChemStation software suite. A Hellma Analytics Excalibur Immersion Probe with a 10 mm path length (Article No. 661-202-10-S-46) was used for variable temperature UV-vis spectroscopic measurements and a standard 1 cm quartz cuvette with an air tight screw cap with a puncturable Teflon seal was used for room temperature measurements. Variable temperature UV-vis spectra were smoothed using the 10 points adjacent averaging function in Origin (OriginLab, Northhampton, MA). ^{1}H and ^{13}C NMR spectra were recorded on a Bruker DRX-400 spectrometer and referenced to residual proteo-solvent peaks. GC-MS data were collected using an Agilent 7890B GC equipped with an Agilent HP-5MS column coupled to an Agilent 5977A EI/PCI-MS. Isotope patterns were compared to the NIST library to confirm assignments. Electrochemical measurements were carried out using a BAS Epsilon potentiostat and using BAS Epsilon software version 1.40.67NT.

Synthesis of 9-phenyl-9H-fluorene

To a solution of lithium diisopropylamide (0.30 mmol made *in situ* from a 1:1 mixture of 2.5 M n-BuLi and diisopropylamine) in THF (3 mL) in the glovebox was added a solution of fluorene (166 mg, 0.10 mmol) in THF (3 mL). The bright orange solution was stirred for 30 minutes at room temperature after which fluorobenzene (141 μL, 0.15 mmol) was added. The resulting dark solution was stirred for 3 hours at room temperature before removal from the glovebox and addition of methanol (1 mL). Ethyl acetate was added to the pale yellow solution which was then washed twice with brine. The organic layer was dried over $MgSO_4$, filtered, and pumped down to a pale yellow solid. Recrystallization from ethanol (EtOH) gave pure 9-phenyl-9*H*-fluorene (90 mg, 37% yield) as a white solid which matched the reported ^{1}H NMR spectrum.[56] ^{1}H NMR ($CDCl_3$, 400 MHz): δ 7.80 (2H, d), 7.41-7.23 (9H, m), 7.10 (2H, d), 5.05 (1H, s).

Synthesis of 9-(4-X-phenyl)-9H-fluorene (X = OMe, Me, or CF_3)

To a solution of 9-fluorenone (0.50 g, 2.8 mmol) in toluene (30 mL) under air was added $TsNHNH_2$ (0.775 g, 4.2 mmol) and the mixture heated at 80 °C for 2 hours. To the bright yellow homogeneous solution was added K_2CO_3 (0.575 g, 4.2 mmol) and 4-X-phenylboronic acid (4.2 mmol). The heterogenous mixture was heated at reflux at 110 °C for 5 hours before cooling to room temperature. Dichloromethane (DCM) and saturated aqueous $NaHCO_3$ were added and the layers separated. The aqueous layer was washed twice with DCM followed by washing the combined organic layers once each with saturated aqueous $NaHCO_3$ and brine. The organic layer was dried with $MgSO_4$, filtered, and pumped down to a yellow solid. Recrystallization from EtOH afforded the desired compounds in pure forms which matched the reported ^{1}H NMR spectra.[57] Yields were 47%, 32%, and 30% for X = OMe, Me, and CF_3, respectively. ^{1}H NMR ($CDCl_3$, 400 MHz, X = OMe): δ 7.78 (2H, d), 7.37 (2H, t), 7.30-7.23 (4H, m), 7.00 (2H, d), 6.82 (2H, d), 5.01 (1H, s), 3.78 (3H, s). ^{1}H NMR ($CDCl_3$, 400 MHz, X = Me): δ 7.78 (2H, d), 7.37 (2H, t), 7.32-7.23 (4H, m), 7.07 (2H, d), 6.99 (2H, d), 5.02 (1H, s), 2.31 (3H, s). ^{1}H NMR ($CDCl_3$, 400 MHz, X = CF_3): δ 7.81 (2H, d), 7.53 (2H, t), 7.41 (2H, m), 7.27 (4H, m), 7.21 (2H, d), 5.10 (1H, s).

Synthesis of 9-(tert-butyl)-9H-fluorene

To a suspension of 9-fluorenone (1.05 g, 5.8 mmol) in 20 mL of hexanes was added a solution of ^{t}BuLi dropwise (1.5 M in pentanes, 6.0 mL). The dark solution was allowed to stir at room temperature overnight after which H_2O (25 mL) was added and the layers separated. The aqueous layer was extracted twice with hexanes and the combined organic layers washed once with H_2O. The organic layer was dried over $MgSO_4$, filtered, and the solvent evaporated. The residue was dissolved in DCM (20 mL) after which Et_3SiH (2 mL) and BF_3•Et_2O (1.6 mL) were added. The resulting homogeneous solution was stirred at room temperature for two days after which H_2O (20 mL) was added. The aqueous layer was extracted twice with DCM and the combined organic layers dried over $MgSO_4$, filtered, and pumped down to an orange residue. The residue was dissolved in hexanes and run through a silica plug to remove orange impurities. The hexanes were removed and the resulting residue

recrystallized from methanol to give the desired product (220 mg, 17% yield) in pure form which matches the reported ^{1}H NMR spectrum.[58] ^{1}H NMR ($CDCl_3$, 400 MHz): δ 7.68 (2H, dt), 7.54 (2H, ddd), 7.33 (2H, tdd), 7.22 (2H, td), 3.63 (1H, s), 1.00 (9H, s).

Synthesis of 1,1,3,3-tetraphenylpropene

1,1-diphenylethylene (353 μL, 2.0 mmol) and benzhydrol (184 mg, 1.0 mmol) were dissolved in DCM (30 mL). p-toluenesulfonic acid (190 mg, 1.1 mmol) and $FeCl_3$•$6H_2O$ (27 mg, 0.01 mmol) were added and the solution heated at reflux for 4 hours. The resulting green solution was cooled to room temperature and the solvent evaporated. The residue was extracted with Et_2O and filtered through silica. Recrystallization from EtOH gave the desired product (289 mg, 83% yield) which matched the reported ^{1}H NMR spectrum.[59] ^{1}H NMR ($CDCl_3$, 400 MHz): δ 7.37-7.15 (20H, m), 6.53 (1H, d), 4.83 (1H, d).

Synthesis of 3-methylxanthene

This synthesis was carried out in two steps. First, the corresponding 3-methylxanthone was made following a modified literature procedure.[60] 2-nitrobenzaldehyde (2.00 g, 13.2 mmol), *m*-cresol (1.86 g, 19.8 mmol), $CuCl_2$ (89 mg, 0.66 mmol), PPh_3 (260 mg, 0.99 mmol), and K_3PO_4•H_2O (6.70 g, 29.0 mmol) were mixed in ~100 mL of dry toluene. The heterogeneous mixture was refluxed at 110 °C under an active flow of N_2, during which it darkened. After cooling to room temperature, ~250 mL of DCM was added and the combined organic layers washed twice with H_2O and once with brine. The organic layers were dried over $MgSO_4$, filtered, and pumped down to a dark residue. This residue was dissolved in pure DCM, washed twice with 1 M NaOH, dried over $MgSO_4$, filtered through silica to remove dark colored impurities, and pumped down to a brown solid. This solid was recrystallized from EtOH to give pure 3-methylxanthone (376 mg, 14% yield) which was carried on into the next step. ^{1}H NMR ($CDCl_3$, 400 MHz): δ 8.35 (1H, dd), 8.22 (1H, d), 7.72 (1H, td), 7.48 (1H, dd), 7.38 (1H, td), 7.30 (1H, s), 7.22 (1H, d), 2.52 (3H, s). A previously reported reduction procedure was used to produce 3-methylxanthene.[61] 3-methylxanthone (300 mg, 1.4 mmol) was dissolved in dry THF. BH_3SMe_2 (1.78 mL of a 2.0 M solution in THF) was added under N_2 and the reaction stirred at room temperature overnight. The THF was removed under vacuum and the residue dissolved in DCM. The organic layer was washed twice with 2 M NaOH and filtered. The filtrate was acidified with concentrated HCl and filtered again. The filtrate was then washed with H_2O, dried over $MgSO_4$, filtered, and pumped down to an off-white powder that was pure 3-methylxanthene (185 mg, 66% yield). The ^{1}H NMR spectrum matched that reported in the literature. ^{1}H NMR ($CDCl_3$, 400 MHz): δ 7.16 (2H, m), 7.03 (3H, m), 6.87 (2H, m), 4.01 (2H, s), 2.32 (3H, s).

Synthesis of fluorene-d_2

Fluorene (250 mg, 1.5 mmol) was dissolved in DMSO-d_6 (~0.8 M) and three equivalents of solid NaH were added. The suspension was stirred for 3-6 hours before addition of excess D_2O. The mixture was extracted with hexanes and the aqueous layer washed again with hexanes. The combined organic layers were washed with H_2O, dried over $MgSO_4$, filtered, and pumped down. The residue was recrystallized from methanol (90 mg, 36% yield). ^{1}H NMR spectroscopy showed 95% deuterium incorporation.[62]

Synthesis of [HMTBD][BF_4]

To a solution of MTBD in Et_2O was added an equimolar amount of HBF_4•Et_2O. The resulting precipitate was collected and dried under vacuum to yield pure [HMTBD][BF_4] (500 mg, 64% yield). ^{1}H NMR (CD_3CN, 400 MHz): δ 5.95 (1H, s, N-H), 3.28 (8H, m, CH_2), 2.88 (3H, s, Me), 1.95 (4H, m, CH_2). ^{13}C NMR (CD_3CN, 100 MHz): δ 151.2, 48.8, 48.3, 47.8, 39.6, 37.5, 21.5, 21.3.

Synthesis of [DMTBD][BF_4]

This was made analogously to [HMTBD][BF_4] described above, but DBF_4 was used instead of HBF_4•Et_2O. The DBF_4 was prepared *in situ* by mixing together HBF_4•Et_2O and D_2O in a 1:3 ratio by volume.[63] The product was recrystallized by layering a THF solution under Et_2O at −35 °C and showed 90% deuterium incorporation at the acidic position by ^{1}H NMR (200 mg, 51% yield).

Titration of PhB(^{t}BuIm)$_3$Co^{III}O with [HMTBD][BF_4]

The titration of **3** with [HMTBD][BF_4] was monitored by ^{1}H NMR spectroscopy. As the product of the reaction, **2**, is unstable above −35 °C, the samples were prepared and stored cold and the spectra were collected at −35 °C. Spectra were collected on three separate samples for each amount of acid added. To prepare a typical sample, 0.25 mL of a 20 mM solution of **3** in CD_3CN was transferred to a J. Young NMR tube. Next, 0.10 mL of a 50 mM solution of hexamethyldisiloxane (TMS_2O) in CD_3CN was added as an internal standard followed by addition of varying volumes of a 50 mM solution of [HMTBD][BF_4] in CD_3CN to reach 0.25, 0.50, 0.75, 1.0, or 1.5 equivalents of added acid relative to **3**. Finally, the samples were diluted with CD_3CN to reach a total volume of 0.50 mL and initial concentrations of 10 mM **3**, 10 mM TMS_2O, and 2.5-15 mM [HMTBD][BF_4]. It was discovered upon collecting the spectra that all species in solution (**2**, **3**, [HMTBD][BF_4], and MTBD) were in rapid equilibrium. The concentration of each species in solution at equilibrium was determined using Equations 2-6 and the observed chemical shift for the methyl protons of MTBD/[HMTBD][BF_4]. From this data the equilibrium constant for the reaction shown in Equation 7, K_{eq}, was calculated and the values obtained from each initial concentration tested averaged. Finally, the relationship shown in Equation 8 was used to calculate the K_a of **2**.

$$\delta_{obs} = \mathrm{X}_{MTBD}\delta_{MTBD} + X_{HMTBD}\delta_{HMTBD} \quad (2)$$

$$[HTMBD]_{eq} = \frac{[HMTBD]_i(\delta_{obs}-\delta_{MTBD})}{\delta_{HMTBD}-\delta_{MTBD}} \quad (3)$$

$$[MTBD]_{eq} = [HMTBD]_i - [HMTBD]_{eq} \quad (4)$$

$$[\mathbf{2}]_{eq} = [MTBD]_{eq} \quad (5)$$

$$[\mathbf{3}]_{eq} = [\mathbf{3}]_i - [\mathbf{2}]_{eq} \quad (6)$$

$$\mathbf{3} + [HMTBD][BF_4] \xrightarrow{K_{eq}} \mathbf{2} + MTBD \quad (7)$$

$$K_{eq} = \frac{K_{a,HMTBD}}{K_{a,2}} \quad (8)$$

Procedure for kinetic studies

Data for rate determination were collected in triplicate at ambient temperature unless otherwise noted. In a typical experiment, 2.0 mL of a 1.25 mM solution of **3** in THF was transferred to an air tight screw top cuvette. After an initial scan (or single absorbance data point at 470 nm) was collected, a solution of substrate in THF was injected through the septum in the screw top. The reaction was monitored for an appropriate amount of time to either reach completion or ~3 half-lives. To determine the observed rate k_{obs} values, the data were analyzed by plotting the natural log of the absorbance at 470 nm at time *t* divided by the initial absorbance vs time in seconds to give k_{obs} as the slope of the linear fit of the data. For diphenylmethane, this plot was generated using the absorbance at 556 nm due to a convoluting absorbance at 470 nm from the radical product generated. To determine the second order rate constants k_2 for various substrates, the k_{obs} values were collected at various concentrations of substrate and plotted vs the substrate concentration to give k_2 as the slope of the linear fit of the data. These k_2 values were used to estimate k_{obs} at 10 equivalents of substrate for diphenylmethane and 1,3-CHD due to the kinetically competitive self-decay rate of **3** at low substrate concentration. KIE values were obtained by evaluating k_H/k_D for DHA and fluorene using the k_{obs} values obtained with 10 equivalents of substrate. Hammett analysis was carried out by comparing the relative rates (k_{obs} obtained using 10 equivalents of substrate) of reaction of the substituted substrates to the unsubstituted 9-phenyl-9*H*-fluorene or xanthene.

Determination of activation parameters for the reaction between 3 and DHA

Data for rate determination were collected in triplicate at each temperature used for the Eyring analysis. In a typical experiment, 4.0 mL of a 1.25 mM solution of **3** in THF was transferred to a custom made, air-tight apparatus equipped with a 14/20 ground glass joint, #2 size ground glass plug, and #25 size threaded Teflon plug for the immersion probe to go through which was sealed with a Teflon coated O-ring. The entire apparatus was sealed inside the glovebox and removed before cooling to the appropriate temperature (10 °C, 0 °C, –10 °C, –20 °C, and –30 °C) under a positive pressure of N_2 through the ground glass plug. After collecting an initial scan, 50 equivalents of DHA were added as a 1.25 M solution in THF (200 μL) injected through a rubber septum in the ground glass joint. The reaction was monitored until ~3 half-lives had been completed. To determine the observed rate k_{obs} values, the data were analyzed by plotting the natural log of the absorbance at 470 nm at time *t* divided by the initial absorbance vs time in seconds to give k_{obs} as the slope of the linear fit of the data. Using the relationship k_{obs} = [DHA]*k_2, the k_2 values were determined at each temperature and a plot of ln(k_2/T) vs 1/T was generated (where T is the temperature in Kelvin). The activation parameters $\Delta H^{\ddagger}$ and $\Delta S^{\ddagger}$ were determined from the linear fit via the Eyring equation (Figure S7, Table 1).

Determination of the upper bound k_{et} for 2 from CV measurements

A 3 mM solution of **1** in MeCN was prepared with 0.1 M $TBAPF_6$ as the electrolyte. A glassy carbon working electrode with a 3 mm diameter was used along with a Pt wire counter electrode and a Ag wire reference electrode that was externally referenced to the Fc/Fc^+ couple. CVs were collected from –964 mV to +235 mV versus Fc/Fc^+ at varying scan rates (10 mV/s, 25 mV/s, 50 mV/s, 75 mV/s, 100 mV/s, 150 mV/s, 200 mV/s, 250 mV/s, 300 mV/s, 400 mV/s, and 800 mV/s). The peak anodic and cathodic current densities, j_p, were plotted versus the square roots of the scan rates ($\nu^{1/2}$). The linear fits of these data were used with Equation 9 (for quasi-reversible electron transfer) to determine the diffusion coefficients, D_R and D_O, respectively, for the reduced (**1**) and oxidized (**2**) species. α was assumed to be 0.5, n = 1 for the single electron transferred, and c is the concentration. The spread in the anodic and cathodic peak potentials (ΔE_p) for each scan rate was converted to the dimensionless parameter Ψ according to Reference 46. Ψ was plotted versus $\nu^{-1/2}$ and the slope of the linear fit of this data was used with Equation 10 to determine k_s. Equation 11 shows the relationship between $\Delta G^{\ddagger}$ and *k*, where *Z* is the collision frequency for the heterogeneous (Z_E, Equation 12, M = the mass of the complex, 533 g/mol) or homogeneous (Z_H, Equation 13, μ = the reduced mass of the reactant pair, 126 g/mol, r = the distance between the reactant pair, 7*10^{-8} cm) process. Assuming that the difference between $\Delta G^{\ddagger}$ for these processes is negligible (see Reference 47), k_{et} can be estimated from k_s using Equation 14. Estimating k_{et} at different temperatures is done using Equation 15 which is derived from Equations 11 and 13 and assumes $\Delta H^{\ddagger} \sim 10$ kcal/mol.

$$j_p = (3 * 10^5) n (n\alpha)^{1/2} D^{1/2} c \nu^{1/2} \quad (9)$$

$$\Psi = \left(\frac{D_O}{D_R}\right)^{\alpha} k_s \left(\frac{\pi D_O n F \nu}{RT}\right)^{-1/2} \quad (10)$$

$$\Delta G^{\ddagger} = -RT \ln\left(\frac{k}{Z}\right) \quad (11)$$

$$Z_E = \left(\frac{RT}{2\pi M}\right)^{1/2} \quad (12)$$

$$Z_H = (6.022 * 10^{20}) \left(\frac{8\pi RT}{\mu}\right)^{1/2} r^2 \quad (13)$$

$$\frac{k_s}{Z_E} = \frac{k_{et}}{Z_H} \quad (14)$$

$$\frac{k_{T_2}}{k_{T_1}} = \left(\frac{T_2}{T_1}\right)^{\frac{1}{2}} e^{\frac{-\Delta H^{\ddagger}}{R}\left(\frac{1}{T_2} - \frac{1}{T_1}\right)} \quad (15)$$

Reaction of 3 and fluorene in the presence of $[DMTBD][BF_4]$ and MTBD at –35 °C

Reactions were carried out in the glovebox on a 1.0 mL scale at –35 °C with the same initial concentrations used for

kinetic measurements (see above). Before addition of substrate, 2.0 equivalents of [DMTBD][BF_4] and 3.2 equivalents of MTBD were added to the solution of **3**. The reactions were left in the freezer for ~24 hours after which they were diluted by a factor of ~10, filtered through silica gel, and analyzed by GC-MS to screen for any deuterium incorporation into aromatic hydrocarbon products.

Evaluation of representative reaction conversion percentages by GC-MS

Reactions were carried out in the glovebox on a 1.0 mL scale with the same initial concentrations used for kinetic measurements (see above). After the reaction was complete, mesitylene was added as an internal standard (0.5 equivalents relative to the initial amount of **3** present). The reaction solutions were then diluted by a factor of 10, passed through silica to remove Co, and analyzed by GC-MS. For analysis of the reaction with DHA, EI-MS was used. For analysis of the reaction with fluorene, PCI-MS was used. Integration of the peaks in the chromatograms and comparison to a calibration curve of pure mesitylene allowed for the determination of the concentration of the products in solution from which the percent conversion was calculated.

Computational methods

Geometry optimizations and numerical frequency calculations were performed using the ORCA program suite.[64] The O3LYP hybrid functional was used for these calculations. The basis sets for each atom were as follows: def2-TZVPP for Co, N, O, the carbene carbons of the ligand, and the carbon undergoing C-H activation in each substrate; def2-SVP for all other atoms. The COSMO solvation model for THF solvation was included in all geometry calculations. A full frequency calculation was performed on each structure to ensure that there were no imaginary frequencies and ensure true minima in the energies. The initial geometries were generated with a simple molecular mechanics geometry optimization in the Hyperchem program suite.[65] The computed energy for each species was corrected for thermal energy contributions. Calculation of pK_a values, E^0 values, and η values were performed analogously to methods reported in Reference 22.

The intrinsic bond orbital (IBO) analysis[52–54] was carried out by scanning the reaction coordinate as a function of O-H distance from 1.8 Å to 0.95 Å. This scan was carried out in the ORCA program suite. Each point's energy was minimized during this scan. For these calculations, the BP86 functional was used with the TZVPP basis set on Co, N, and O and 6-31G on the remaining atoms. The results from this scan were examined in the IboView software (http://www.iboview.org/index.html). The orbitals involved in the reaction were identified by analysis of the orbitals along the reaction coordinate (Figure S29). Orbital movement was normalized versus the starting and endpoints of the overall orbital movement.

ASSOCIATED CONTENT

Supporting Information

This material is available free of charge via the Internet at http://pubs.acs.org.

Supplementary derivations, figures, tables, and schemes (PDF)

AUTHOR INFORMATION

Corresponding Author

*E-mail: jsanderson@uchicago.edu

Author Contributions

The manuscript was written through contributions of all authors. All authors have given approval to the final version of the manuscript.

Notes

The authors declare no competing financial interests.

ACKNOWLEDGMENT

Work presented here was funded by the following sources: NSF CAREER award Grant No. 1654144, and the University of Chicago. We are grateful for the support of the University of Chicago Research Computing Center for assistance with the calculations carried out in this work. We would also like to acknowledge Dr. Ethan Hill for encouraging us to think about basicity, Dr. Jonathan H. Skone for many helpful discussions about DFT calculations, Professor Vlad M. Iluc for the insightful suggestion of the deuterium crossover experiment, and Professor Gerald Knizia for his insight regarding IBO analysis.

REFERENCES

(1) Rittle, J.; Green, M. T. "Cytochrome P450 Compound I: Capture, Characterisation, and C-H Bond Activation Kinetics." *Science.* **2010**, *330*, 933–937.

(2) Que, L. "The Road to Non-Heme Oxoferryls and Beyond." *Acc. Chem. Res.* **2007**, *40* (7), 493–500.

(3) Nam, W.; Lee, Y.-M.; Fukuzumi, S. "Hydrogen Atom Transfer Reactions of Mononuclear Nonheme Metal–Oxygen Intermediates." *Acc. Chem. Res.* **2018**, *51* (9), 2014–2022.

(4) Gunay, A.; Theopold, K. H. "C-H Bond Activations by Metal Oxo Compounds." *Chem. Rev.* **2010**, *110* (2), 1060–1081.

(5) Wang, B.; Lee, Y.-M.; Tcho, W.-Y.; Tussupbayev, S.; Kim, S.-T.; Kim, Y.; Seo, M. S.; Cho, K.-B.; Dede, Y.; Keegan, B. C.; Ogura, T.; Kim, S. H.; Ohta, T.; Baik, M.-H.; Ray, K.; Shearer, J.; Nam, W. "Synthesis and Reactivity of a Mononuclear Non-Haem Cobalt(IV)-Oxo Complex." *Nat. Commun.* **2017**, *8*, 14839.

(6) White, M. C.; Zhao, J. "Aliphatic C–H Oxidations for Late-Stage Functionalization." *J. Am. Chem. Soc.* **2018**, *140* (43), 13988–14009.

(7) Sun, C.-L.; Li, B.-J.; Shi, Z.-J. "Direct C–H Transformation via Iron Catalysis." *Chem. Rev.* **2011**, *111* (3), 1293–1314.

(8) Milan, M.; Salamone, M.; Costas, M.; Bietti, M. "The Quest for Selectivity in Hydrogen Atom Transfer Based Aliphatic C–H Bond Oxygenation." *Acc. Chem. Res.* **2018**, *51* (9), 1984–1995.

(9) Warren, J. J.; Tronic, T. A.; Mayer, J. M. "Thermochemistry of Proton-Coupled Electron Transfer Reagents and Its Implications." *Chem. Rev.* **2010**, *110* (12), 6961–7001.

(10) Weinberg, D. R.; Gagliardi, C. J.; Hull, J. F.; Murphy, C. F.; Kent, C. A.; Westlake, B. C.; Paul, A.; Ess, D. H.; McCafferty, D. G.; Meyer, T. J. "Proton-Coupled Electron Transfer." *Chem. Rev.* **2012**, *112* (7), 4016–4093.

(11) Huynh, M. H. V.; Meyer, T. J. "Proton-Coupled Electron Transfer." *Chem. Rev.* **2007**, *107* (11), 5004–5064.

(12) Cukier, R. I.; Nocera, D. G. "Proton-Coupled Electron Transfer." *Annu. Rev. Phys. Chem.* **1998**, *49* (1), 337–369.

(13) Mayer, J. M. "Understanding Hydrogen Atom Transfer: From Bond Strengths to Marcus Theory." *Acc. Chem. Res.* **2011**, *44* (1), 36–46.

(14) Bell, R. P. "The Theory of Reactions Involving Proton Transfers." *Proc. R. Soc. A Math. Phys. Eng. Sci.* **1936**, *154* (882), 414–429.

(15) Evans, M. G.; Polanyi, M. "Inertia and Driving Force of Chemical Reactions." *Trans. Faraday Soc.* **1938**, *34*, 11–24.

(16) Zaragoza, J. P. T.; Siegler, M. A.; Goldberg, D. P. "A Reactive Manganese(IV)-Hydroxide Complex: A Missing Intermediate in Hydrogen Atom Transfer by High-Valent Metal-Oxo

Porphyrinoid Compounds." *J. Am. Chem. Soc.* **2018**, *140* (12), 4380–4390.
(17) Lansky, D. E.; Goldberg, D. P. "Hydrogen Atom Abstraction by a High-Valent Manganese(V)−Oxo Corrolazine." *Inorg. Chem.* **2006**, *45*, 5119–5125.
(18) McDonald, A. R.; Que, L. "High-Valent Nonheme Iron-Oxo Complexes: Synthesis, Structure, and Spectroscopy." *Coord. Chem. Rev.* **2013**, *257* (2), 414–428.
(19) Sastri, C. V; Lee, J.; Oh, K.; Lee, Y. J.; Lee, J.; Jackson, T. A.; Ray, K.; Hirao, H.; Shin, W.; Halfen, J. A.; Kim, J.; Que, L.; Shaik, S.; Nam, W. "Axial Ligand Tuning of a Nonheme Iron(IV) Oxo Unit for Hydrogen Atom Abstraction." *Proc. Natl. Acad. Sci.* **2007**, *104* (49), 19181–19186.
(20) Dhar, D.; Tolman, W. B. "Hydrogen Atom Abstraction from Hydrocarbons by a Copper(III)-Hydroxide Complex." *J. Am. Chem. Soc.* **2015**, *137* (3), 1322–1329.
(21) Usharani, D.; Lacy, D. C.; Borovik, A. S.; Shaik, S. "Dichotomous Hydrogen Atom Transfer vs Proton-Coupled Electron Transfer During Activation of X–H Bonds (X = C, N, O) by Nonheme Iron–Oxo Complexes of Variable Basicity." *J. Am. Chem. Soc.* **2013**, *135* (45), 17090–17104.
(22) Bím, D.; Maldonado-Domínguez, M.; Rulíšek, L.; Srnec, M. "Beyond the Classical Thermodynamic Contributions to Hydrogen Atom Abstraction Reactivity." *Proc. Natl. Acad. Sci.* **2018**, *115* (44), E10287–E10294.
(23) Hodgkiss, J. M.; Rosenthal, J.; Nocera, D. G. The Relation between Hydrogen Atom Transfer and Proton-Coupled Electron Transfer in Model Systems. In *Hydrogen-Transfer Reactions*; Hynes, J. T., Klinman, J. P., Limbach, H.-H., Schowen, R. L., Eds.; WILEY-VCH Verlag GmbH: Weinheim, 2007; pp 503–562.
(24) Hammes-Schiffer, S. "Theory of Proton-Coupled Electron Transfer in Energy Conversion Processes." *Acc. Chem. Res.* **2009**, *42* (12), 1881–1889.
(25) Fulton, J. R.; Sklenak, S.; Bouwkamp, M. W.; Bergman, R. G. "A Comprehensive Investigation of the Chemistry and Basicity of a Parent Amidoruthenium Complex." *J. Am. Chem. Soc.* **2002**, *124* (17), 4722–4737.
(26) Roth, J. P.; Mayer, J. M. "Hydrogen Transfer Reactivity of a Ferric Bi-Imidazoline Complex That Models the Activity of Lipoxygenase Enzymes." *Inorg. Chem.* **1999**, *38* (12), 2760–2761.
(27) Parsell, T. H.; Yang, M. Y.; Borovik, A. S. "C-H Bond Cleavage with Reductants: Re-Investigating the Reactivity of Monomeric $Mn^{III/IV}$-Oxo Complexes and the Role of Oxo Ligand Basicity." *J. Am. Chem. Soc.* **2009**, *131* (8), 2762–2763.
(28) Zdilla, M. J.; Dexheimer, J. L.; Abu-Omar, M. M. "Hydrogen Atom Transfer Reactions of Imido Manganese(V) Corrole: One Reaction with Two Mechanistic Pathways." *J. Am. Chem. Soc.* **2007**, *129* (37), 11505–11511.
(29) Yosca, T. H.; Rittle, J.; Krest, C. M.; Onderko, E. L.; Silakov, A.; Calixto, J. C.; Behan, R. K.; Green, M. T. "Iron(IV)Hydroxide PK(a) and the Role of Thiolate Ligation in C-H Bond Activation by Cytochrome P450." *Science.* **2013**, *342* (6160), 825–829.
(30) Green, M. T.; Dawson, J. H.; Gray, H. B. "Oxoiron(IV) in Chloroperoxidase Compound II Is Basic: Implications for P450 Chemistry." *Science.* **2004**, *304* (5677), 1653–1656.
(31) Donoghue, P. J.; Tehranchi, J.; Cramer, C. J.; Sarangi, R.; Solomon, E. I.; Tolman, W. B. "Rapid C–H Bond Activation by a Monocopper(III)–Hydroxide Complex." *J. Am. Chem. Soc.* **2011**, *133* (44), 17602–17605.
(32) Dhar, D.; Yee, G. M.; Markle, T. F.; Mayer, J. M.; Tolman, W. B. "Reactivity of the Copper(III)-Hydroxide Unit with Phenols." *Chem. Sci.* **2017**, *8* (2), 1075–1085.
(33) Goetz, M. K.; Hill, E. A.; Filatov, A. S.; Anderson, J. S. "Isolation of a Terminal Co(III)-Oxo Complex." *J. Am. Chem. Soc.* **2018**, *140* (41), 13176–13180.
(34) Kaljurand, I.; Kütt, A.; Sooväli, L.; Rodima, T.; Mäemets, V.; Leito, I.; Koppel, I. A. "Extension of the Self-Consistent Spectrophotometric Basicity Scale in Acetonitrile to a Full Span of 28 pK_a Units: Unification of Different Basicity Scales." *J. Org. Chem.* **2005**, *70* (3), 1019–1028.
(35) Lacy, D. C.; Gupta, R.; Stone, K. L.; Greaves, J.; Ziller, J. W.; Hendrich, M. P.; Borovik, A. S. "Formation, Structure, and EPR Detection of a High Spin Fe^{IV}-Oxo Species Derived from Either an Fe^{III}-Oxo or Fe^{III}-OH Complex." *J. Am. Chem. Soc.* **2010**, *132* (35), 12188–12190.
(36) Bryant, J. R.; Mayer, J. M. "Oxidation of C–H Bonds by $[(Bpy)_2(Py)Ru^{IV}O]^{2+}$ Occurs by Hydrogen Atom Abstraction." *J. Am. Chem. Soc.* **2003**, *125* (34), 10351–10361.
(37) Lebeau, E. L.; Binstead, R. A.; Meyer, T. J. "Mechanistic Implications of Proton Transfer Coupled to Electron Transfer." *J. Am. Chem. Soc.* **2001**, *123* (43), 10535–10544.
(38) Jeong, Y. J.; Kang, Y.; Han, A.-R.; Lee, Y.-M.; Kotani, H.; Fukuzumi, S.; Nam, W. "Hydrogen Atom Abstraction and Hydride Transfer Reactions by Iron(IV)-Oxo Porphyrins." *Angew. Chem., Int. Ed.* **2008**, *47* (38), 7321–7324.
(39) Caldin, E. F. "Tunneling in Proton-Transfer Reactions in Solution." *Chem. Rev.* **1969**, *69* (1), 135–156.
(40) Cong, Z.; Kinemuchi, H.; Kurahashi, T.; Fujii, H. "Factors Affecting Hydrogen-Tunneling Contribution in Hydroxylation Reactions Promoted by Oxoiron(IV) Porphyrin π-Cation Radical Complexes." *Inorg. Chem.* **2014**, *53* (19), 10632–10641.
(41) Mandal, D.; Mallick, D.; Shaik, S. "Kinetic Isotope Effect Determination Probes the Spin of the Transition State, Its Stereochemistry, and Its Ligand Sphere in Hydrogen Abstraction Reactions of Oxoiron(IV) Complexes." *Acc. Chem. Res.* **2018**, *51* (1), 107–117.
(42) Edwards, S. J.; Soudackov, A. V; Hammes-Schiffer, S. "Analysis of Kinetic Isotope Effects for Proton-Coupled Electron Transfer Reactions." *J. Phys. Chem. A* **2009**, *113* (10), 2117–2126.
(43) Bordwell, F. G. "Equilibrium Acidities in Dimethyl Sulfoxide Solution." *Acc. Chem. Res* **1988**, *21* (7), 456–463.
(44) Luo, Y.-R. "Handbook of Bond Dissociation Energies in Organic Compounds;" CRC Press: Boca Raton, 2003.
(45) Hansch, C.; Leo, A.; Taft, R. W. "A Survey of Hammett Substituent Constants and Resonance and Field Parameters." *Chem. Rev.* **1991**, *91* (2), 165–195.
(46) Nicholson, R. S. "Theory and Application of Cyclic Voltammetry for Measurement of Electrode Reaction Kinetics." *Anal. Chem.* **1965**, *37* (11), 1351–1355.
(47) Klingler, R. J.; Kochi, J. K. "Electron-Transfer Kinetics from Cyclic Voltammetry. Quantitative Description of Electrochemical Reversibility." *J. Phys. Chem.* **1981**, *85* (12), 1731–1741.
(48) Bryant, R. G. "The NMR Time Scale." *J. Chem. Educ.* **1983**, *60* (11), 933–935.
(49) Klinker, E. J.; Shaik, S.; Hirao, H.; Que, L. "A Two-State Reactivity Model Explains Unusual Kinetic Isotope Effect Patterns in C-H Bond Cleavage by Nonheme Oxoiron(IV) Complexes." *Angew. Chem., Int. Ed.* **2009**, *48* (7), 1291–1295.
(50) Mandal, D.; Mallick, D.; Shaik, S. "Kinetic Isotope Effect Determination Probes the Spin of the Transition State, Its Stereochemistry, and Its Ligand Sphere in Hydrogen Abstraction Reactions of Oxoiron(IV) Complexes." *Acc. Chem. Res.* **2018**, *51* (1), 107–117.
(51) Hickey, A. K.; Lutz, S. A.; Chen, C.-H.; Smith, J. M. "Two-State Reactivity in C–H Activation by a Four-Coordinate Iron(0) Complex." *Chem. Commun.* **2017**, *53* (7), 1245–1248.
(52) Knizia, G. "Intrinsic Atomic Orbitals: An Unbiased Bridge between Quantum Theory and Chemical Concepts." *J. Chem. Theory Comput.* **2013**, *9* (11), 4834–4843.
(53) Knizia, G.; Klein, J. E. M. N. "Electron Flow in Reaction Mechanisms-Revealed from First Principles." *Angew. Chem., Int. Ed.* **2015**, *54* (18), 5518–5522.
(54) Klein, J. E. M. N.; Knizia, G. "CPCET versus HAT: A Direct Theoretical Method for Distinguishing X-H Bond-Activation Mechanisms." *Angew. Chem., Int. Ed.* **2018**, *57* (37), 11913–11917.
(55) Goldsmith, C. R.; Jonas, R. T.; Stack, T. D. P. "C-H Bond Activation by a Ferric Methoxide Complex: Modeling the Rate-Determining Step in the Mechanism of Lipoxygenase." *J. Am. Chem. Soc.* **2002**, *124* (1), 83–96.
(56) Ji, X.; Huang, T.; Wu, W.; Liang, F.; Cao, S. "LDA-Mediated Synthesis of Triarylmethanes by Arylation of Diarylmethanes with Fluoroarenes at Room Temperature." *Org. Lett.* **2015**, *17* (20), 5096–5099.
(57) Shen, X.; Gu, N.; Liu, P.; Ma, X.; Xie, J.; Liu, Y.; He, L.; Dai, B. "A

Simple and Efficient Synthesis of 9-Arylfluorenes via Metal-Free Reductive Coupling of Arylboronic Acids and N-Tosylhydrazones in Situ." *RSC Adv.* **2015**, *5* (78), 63726–63731.

(58) Li, H.; Aquino, A. J. A.; Cordes, D. B.; Hung-Low, F.; Hase, W. L.; Krempner, C. "A Zwitterionic Carbanion Frustrated by Boranes - Dihydrogen Cleavage with Weak Lewis Acids via an 'Inverse' Frustrated Lewis Pair Approach." *J. Am. Chem. Soc.* **2013**, *135* (43), 16066–16069.

(59) Liu, Z. Q.; Zhang, Y.; Zhao, L.; Li, Z.; Wang, J.; Li, H.; Wu, L. M. "Iron-Catalyzed Stereospecific Olefin Synthesis by Direct Coupling of Alcohols and Alkenes with Alcohols." *Org. Lett.* **2011**, *13* (9), 2208–2211.

(60) Hu, J.; Adogla, E. A.; Ju, Y.; Fan, D.; Wang, Q. "Copper-Catalyzed Ortho-Acylation of Phenols with Aryl Aldehydes and Its Application in One-Step Preparation of Xanthones." *Chem. Commun.* **2012**, *48* (91), 11256.

(61) Stopka, T.; Marzo, L.; Zurro, M.; Janich, S.; Würthwein, E.-U.; Daniliuc, C. G.; Alemán, J.; Mancheño, O. G. "Oxidative C-H Bond Functionalization and Ring Expansion with $TMSCHN_2$: A Copper(I)-Catalyzed Approach to Dibenzoxepines and Dibenzoazepines." *Angew. Chem., Int. Ed.* **2015**, *54* (17), 5049–5053.

(62) Franz, J. A.; Alnajjar, M. S.; Barrows, R. D.; Kaisaki, D. L.; Camaioni, D. M.; Suleman, N. K. "Reactions of the 2-Allylbenzyl Radical: Relative and Absolute Rate Constants for Abstraction of Hydrogen Atom from Thiophenol, Dicyclohexylphosphine, Phenols, and Arylalkyl Donors." *J. Org. Chem.* **1986**, *51* (9), 1446–1456.

(63) Jia, G.; Morris, R. H. "Wide Range of pK_a Values of Coordinated Dihydrogen. Synthesis and Properties of Some η^2-Dihydrogen and Dihydride Complexes of Ruthenium." *J. Am. Chem. Soc.* **1991**, *113* (3), 875–883.

(64) Neese, F. "The Orca Program System." *Wiley Interdiscip. Rev. Mol. Sci.* **2012**, *2*, 73–78.

(65) "HyperChem(TM) Professional 7.51." Hypercube, Inc.: 1115 NW 4th Street, Gainesville, Florida 32601, USA.

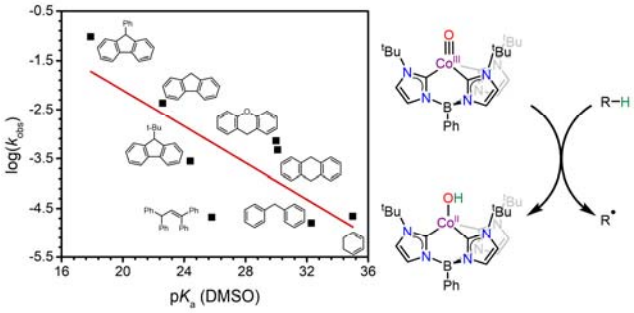

Experimental Evidence for Asynchronous pK_a-Driven C-H Activation